arXiv:chao-dyn/9610013v1 14 Oct 1996

How Chaotic is the Stadium Billiard? A Semiclassical Analysis

Gregor Tanner*
Niels Bohr Institute, Blegdamsvej 17,
DK-2100 Copenhagen Ø, Denmark

September 26, 1996

Abstract

The impression gained from the literature published to date is that the spectrum of the stadium billiard can be adequately described, semiclassically, by the Gutzwiller periodic orbit trace formula together with a modified treatment of the marginally stable family of bouncing ball orbits. I show that this belief is erroneous. The Gutzwiller trace formula is not applicable for the phase space dynamics near the bouncing ball orbits. Unstable periodic orbits close to the marginally stable family in phase space cannot be treated as isolated stationary phase points when approximating the trace of the Green function. Semiclassical contributions to the trace show an $\hbar$ – dependent transition from hard chaos to integrable behavior for trajectories approaching the bouncing ball orbits. A whole region in phase space surrounding the marginal stable family acts, semiclassically, like a stable island with boundaries being explicitly $\hbar$–dependent. The localized bouncing ball states found in the billiard derive from this semiclassically stable island. The bouncing ball orbits themselves, however, do not contribute to individual eigenvalues in the spectrum. An EBK–like quantization of the regular bouncing ball eigenstates in the stadium can be derived. The stadium billiard is thus an ideal model for studying the influence of almost regular dynamics near marginally stable boundaries on quantum mechanics. This behavior is generically found at the border of classically stable islands in systems with a mixed phase space structure.

PACS numbers: 05.45, 03.65.Sq

1 Introduction

The derivation of semiclassical periodic orbit formulas for the trace of the quantum Green function led to a deeper understanding of the influence of classical dynamics on quantum spectra. Closed periodic orbit expressions have been given by Gutzwiller [1] and Balian and Bloch [2] for "hard chaos" systems and by Berry and Tabor [3, 4] for integrable dynamics. Integrability and hard chaos represent the two extremes on the scale of possible Hamiltonian dynamics. The term "hard chaos" introduced by Gutzwiller [1] is, however, not well defined. It implies, that all periodic orbits are unstable and "sufficiently" isolated to allow for the stationary phase approximations in the derivation of the trace formula. Hence, for lack of a better definition, one might say that a system exhibits "hard chaos" if the Gutzwiller trace formula as it stands is the leading term in a semiclassical expansion in $\hbar$.

*email: tanner@kaos.nbi.dk

Neither integrability nor hard chaos is generic in low dimensional bounded Hamiltonian dynamics. The variety of classical systems proposed as testing models for the Gutzwiller trace formula in the last decade exemplify the problem of finding ideal chaos in the sense described above. Typical Hamiltonian systems show a mixture of the two extremes. Chaotic regions in phase space (containing unstable periodic orbits only) are interspersed by stable islands, which themselves may have a complicated inner structure consisting of chaotic bands and invariant tori. The "stable regions" reflect locally almost integrable behavior in phase space and can be treated semiclassically by an Einstein–Brillouin–Keller (EBK) approximation [1, 5, 6]. Semiclassical contributions to the trace of the Green function from periodic orbits inside the stable islands are of modified Berry–Tabor–type as has been discussed in [7, 8, 9, 10, 11].

Much less is known about a semiclassical treatment of the transition region from the stable island to the outer chaotic neighborhood. The outer boundary acts as a classically impenetrable wall in two degrees of freedom. A coupling between dynamically separated regions can only be described by complex trajectories [2, 12, 13]. Although the outer chaotic region contains (per definition) only unstable periodic orbits, it shows almost regular behavior near the stable components. The characteristics for this kind of regularity, also called intermittency in the chaos literature [14], is a vanishing Liapunov exponent λ_p for unstable periodic orbits approaching the island, i.e.

$$\lambda_p = \frac{\log \Lambda_p}{T_p} \underset{T_p \to \infty}{\longrightarrow} 0,$$

where Λ_p denotes the largest eigenvalue of the stability matrix (describing the linearized dynamics in the neighborhood of the periodic orbit) and T_p is the period.

I will show that intermittency in bounded systems leads to leading order corrections in the Gutzwiller trace formula. Semiclassical contributions from (unstable) periodic orbits approaching the boundary of a stable island show a $\hbar$–dependent transition from Gutzwiller to Berry – Tabor like behavior. This allows one to extend the concept of EBK–quantization from a stable region over the marginal stable boundary into its "chaotic" neighborhood.

We will derive these results for a specific example, the quarter stadium billiard, (see Fig. 2). This might appear surprising on first sight, because this billiard has been introduced as an example of a dynamical system which is completely ergodic with positive Liapunov exponent [15]. The stadium billiard has thus been regarded as an ideal model for a "chaotic" system. First indications for the validity of the random matrix conjecture relating the level statistics of individual "chaotic" systems to those of an ensemble of random Gaussian orthogonal matrices have been found in this billiard [16, 17, 18]. Also the discovery of scarred wave functions [19] was first made in this system. From then on, the classical and quantum aspects of the stadium billiard were studied intensively both theoretically and in microwave experiments [20, 21], making it a standard model in quantum chaology. The billiard dynamics possesses, however, regularities, which prevents it from being a hard chaos system. The so–called bouncing ball orbits, i.e. the continuous family of periodic orbits running back and forth in the rectangle, are marginally stable. Another peculiarity of the stadium is the existence of whispering gallery orbits accumulating at the boundary of the billiard. These orbits have a strong, non–generic influence on the spectral statistics which causes deviations from the GOE–predictions [21]. There also exist quantum eigenstates, which are localized along the bouncing ball orbits (the bouncing ball states), or along the boundary (the whispering gallery states), in a much more pronounced way than the scars found along other periodic orbits.

As a consequence, the stadium billiard is not an example of a hard chaos billiard, but may

serve as an ideal model for systems exhibiting both regular and chaotic dynamics. Though there is no stable island, the bouncing ball orbits act as the boundary of a torus enclosing an area with zero volume in phase space. This allows us to study pure boundary effects without dealing with the inner structure of the island.

Semiclassical results obtained for hard chaos systems suffer considerable changes when dealing with intermittency as will be shown here. First of all, the contributions of the marginal stable family to the trace of the Green function need a special treatment [22, 23]. This is true, however, also for unstable periodic orbits close to the bouncing ball family. They can no longer be treated as isolated stationary phase points when approximating the trace of the Green function at finite $\hbar$. As a consequence, the Gutzwiller periodic orbit formula is not valid for the dynamics in a whole phase space volume surrounding the marginal stable family. The size of this volume is explicitly $\hbar$ dependent and shrinks to zero in the semiclassical limit.

Furthermore, standard semiclassical arguments referring to a cut–off in periodic orbit sums at a period given by the Heisenberg time are not valid for intermittent systems. Intermittency is related to a loss of internal time scales in the dynamics and infinitely long orbits thus contribute dominantly to the semiclassical zeta function at finite $\hbar$. In particular, the regular bouncing ball states follow scaling laws for a cut–off in the orbit summation different from the estimate given by the Berry – Keating resummation technique [24].

The article is organized as follows: in section 2, the contribution of the bouncing ball family to the trace of the Green function is discussed. The derivation follows mainly the ideas developed in [22, 23] although here we do not deal with diffraction effects. It will be shown that the bouncing ball orbits give no contribution to individual eigenvalues of the stadium billiard. In section 3, the Bogomolny transfer operator method [26] is introduced. A Poincaré surface of section is defined, which allows us to study the near bouncing ball dynamics, but explicitly excludes the bouncing ball family. The Poincaré map in the bouncing ball limit is derived, which allows us to obtain the leading contributions to the transfer operator for the bouncing ball spectrum. An approximate EBK–quantization of the bouncing ball states can be derived. An analysis of the trace of the transfer operator unveils the breakdown of the Gutzwiller periodic orbit formula for unstable periodic orbits close to the bouncing ball family. In section 4, we develop the concept of a "semiclassical island of stability" surrounding the marginally stable bouncing ball family in phase space and discuss the semiclassical limit of the bouncing ball spectrum.

2 The bouncing ball orbits

In this section, the bouncing ball contribution to the quantum spectral determinant

$$D(E) = \exp \int_0^E dE' \mathrm{Tr} G(E') = \prod_n (E - E_n) \tag{1}$$

is derived. The $\{E_n\}$ denote the real quantum eigenvalues of the system. Following Ref. [22, 23], the Green function for the quarter stadium billiard, Fig. 2, is divided into a bouncing ball part and the rest,

$$G(q, q', k) = G_{bb}(q, q', k) + G_r(q, q', k), \tag{2}$$

where $k = \sqrt{2mE}/\hbar$. The bouncing ball contribution is restricted to q, q' inside the rectangle and contains in semiclassical approximation all paths from q to q' not reaching the circle boundary or bouncing off the vertical line in the rectangle. The classical paths correspond essentially to

free motion, and the bouncing ball Green function G_{bb} can be written as an infinite sum over Hankel functions (plus phases due to hard wall reflections). The trace then has the form [22]

$$\mathrm{Tr}G_{bb}(k) = g_{bb}(k) = -i\frac{ab}{2}k + i\frac{a}{2} - iabk\sum_{n=1}^{\infty} H_0^{(1)}(2bkn) + \lim_{\epsilon\to 0}\frac{abk}{2}N_0(\epsilon k), \tag{3}$$

where a is the length of the rectangle, b denotes the radius of the circle and $H_0^{(1)}$ is the Hankel function of the first kind. The real part of the trace diverges due to the logarithmic singularity of the Neumann function N_0 at the origin. This kind of divergence is a well known phenomenon for the trace of Green functions and can be regularised e.g. by defining $\tilde{g}_{bb}(E) = g_{bb}(E) - \mathrm{Re}[g_{bb}(E_0)]$ for E_0 fixed [27, 28]. Note, that the same regularisation techniques have to be applied for the true quantum trace $g(E) = \sum_n (E - E_n)^{-1}$ and are thus not an artifact of the semiclassical approximation. We now move directly to the integrated trace, which reads

$$\begin{aligned} Ig_{bb}(k) = \int_0^k dk' \tilde{g}_{bb}(k') &= B_{bb}(k^2) - i\pi\overline{N}_{bb}(k) - i\frac{ak}{2}\sum_{n=1}^{\infty}\frac{1}{n}H_1^{(1)}(2kbn). &(4)\\ &\approx B_{bb}(k^2) - i\pi\overline{N}_{bb}(k) - i\frac{a}{2}\sqrt{\frac{k}{\pi b}}\sum_{n=1}^{\infty}\frac{1}{n^{3/2}}e^{2ikbn-\frac{3}{4}i\pi}, &(5)\end{aligned}$$

and the asymptotic form of the Hankel function has been used in the last step. The sum in (5) is of the same kind as the contribution of a periodic orbit family in an integrable system (here the rectangle) as derived by Berry and Tabor [3, 29]. The real part of the non–oscillating contribution is a function of k^2 only,

$$B_{bb}(k^2) = \frac{ab}{4\pi}k^2(\log k^2 - 1) + \frac{ab}{2}\beta k^2 + \frac{a}{b}\frac{\pi}{12}. \tag{6}$$

The real parameter β originates from the regularisation and has the form

$$\beta = -\frac{\log k_0}{\pi} - \sum_{n=1}^{\infty} N_0^{(1)}(2bk_0n) \qquad \text{with} \quad k_0 = \sqrt{2mE_0}\hbar. \tag{7}$$

The imaginary part is the bouncing ball contribution to the mean level staircase function

$$\overline{N}_{bb}(k) = \frac{ab}{4\pi}k^2 - \frac{2a}{4\pi}k. \tag{8}$$

The term $B_{bb}(k^2)$ is of the general form as derived in [28] for arbitrary billiards with compact domain, i.e.

$$B(k^2) = \frac{A}{4\pi}k^2(\log k^2 - 1) + \beta k^2 + \gamma\log k^2 + c, \tag{9}$$

where A corresponds to the volume of the billiard and β, γ, c are real constants. Note, that the logarithmic singularity for $k \to 0$ in (9) is absent in (6). The sum in (4) is convergent on the whole complex k–plane (after analytic continuation for $Im(k) < 0$). The function $Ig_{bb}(k)$ is free of singularities and analytic everywhere apart from the lines $Re(k) = m\pi/b$, m integer, where it exhibits square – root cusps. The dominant oscillation introduced through the bouncing ball orbits is clearly visible in the oscillatory part of the level staircase function [21, 23], and agrees with the prediction (4). The bouncing ball part does, however, not contribute to individual eigenvalues. The spectral determinant (1) can be factorised according to

$$D(k) \approx D_{bb}(k)D_r(k) \qquad \text{with} \quad D_{bb}(k) = e^{Ig_{bb}(k)}, \tag{10}$$

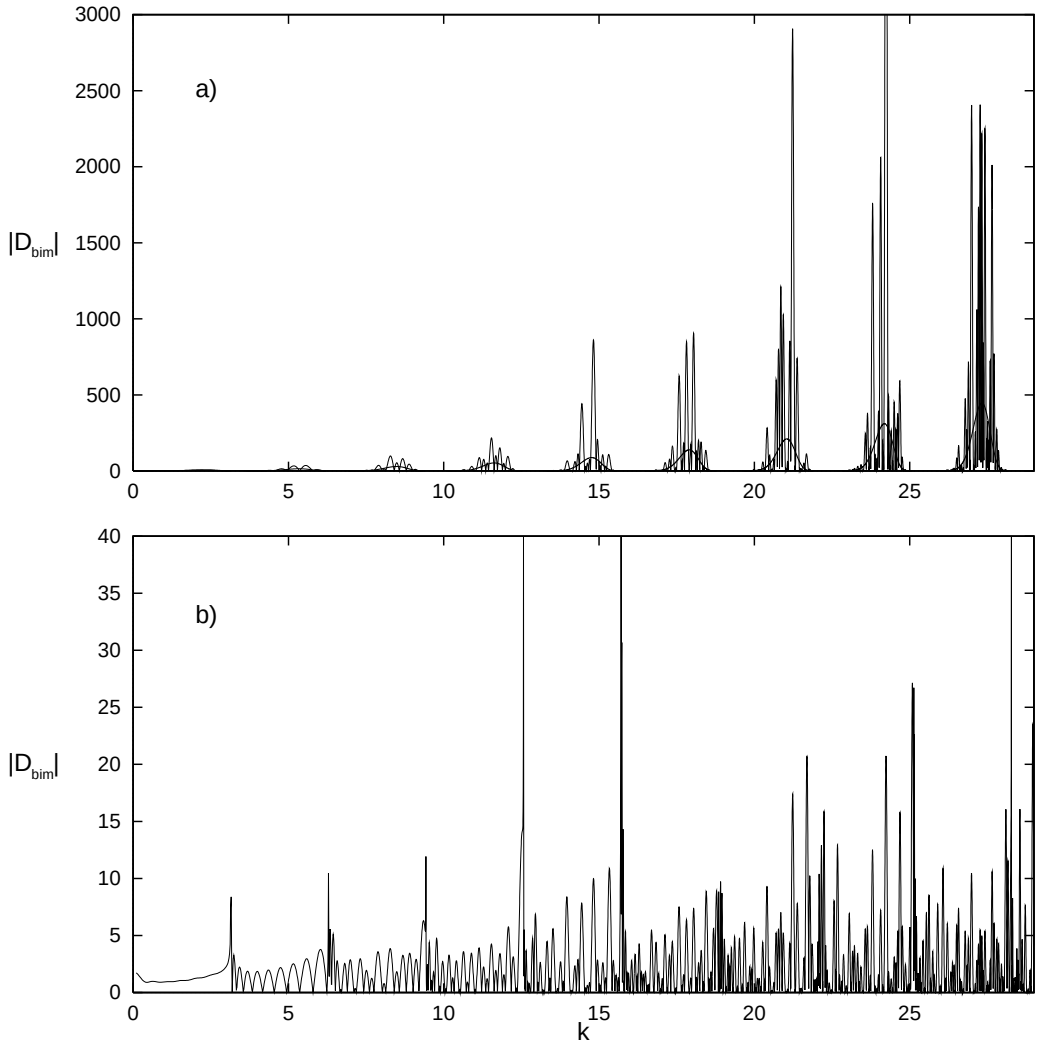

Figure 1: The modulus of the boundary integral spectral determinant before (a) and after (b) dividing out the bouncing ball part, Eqn. (10), here for $a = 5$, $b = 1$; (in addition $D_{bb}(k)$ is plotted in (a)). The k – interval shown contains about 370 energy levels, which are the real zeros of the spectral determinant.

and the bouncing ball contribution $D_{bb}(k)$ is a function which has no zeros in the whole complex k plane. It gives rise to oscillations in the modulus of the spectral determinant with an amplitude growing like $\exp\left(\frac{a}{2}\sqrt{\frac{k}{\pi b}}\right)$ and a period π/b, but it does not influence the individual zeros. The bouncing ball contributions to the spectral determinant can thus be divided out without losing information about the spectrum. This can be demonstrated by considering the boundary integral determinant

$$D_{bim}(k) = \det(\mathbf{1} - \mathbf{K}(q, q', k)), \tag{11}$$

where $\mathbf{K}$ is the boundary integral kernel defined for q and q' on the boundary of the billiard, (for details see [30]). The function $D_{bim}(k)$ has the same zeros as the exact spectral determinant $D(k)$, but may differ otherwise. Especially, a smooth part $\exp(B(k^2) - i\pi\overline{N}(k))$ is absent in the boundary integral determinant. This term originates from the zero length limit in the Green function and is thus a pure volume effect. The modulation due to the bouncing ball contribution is clearly present in $D_{bim}(k)$, see Fig. 1a. The large overall oscillation of the amplitude covers 7 order of magnitudes for $k \approx 30$ but is completely removed by factorising out the bouncing ball part $D_{bb}(k)$, see fig. 1b. Note, that the boundary integral determinant after factorization exhibits cusps at $k = m\pi/b$, and is thus non–analytic there.

As a somewhat paradoxical result, we obtain that the bouncing ball family is responsible for strong modulations in the trace as well as in the spectral determinant. It does not, however, contribute to individual eigenvalues, and does not explain the regular modulation in the level spacing itself. The bouncing ball family covers a volume of measure zero in phase space, and is not sufficient to form a support for an eigenfunction alone. (This is of course true for any invariant family e.g. in an integrable system.) As a consequence, the neighborhood of the bouncing ball family in phase space must be responsible for the existence of the bouncing ball states and for the periodic change in the level spacings leading to the modulation in the level staircase function. The next section is devoted to a proper semiclassical analysis of the near bouncing ball dynamics.

3 The semiclassical transfer operator

So far, it has been widely believed, that the remainder term in the trace of the Green function (2) as well as in the spectral determinant (10) can in leading semiclassical approximation be described by the Gutzwiller periodic orbit formula [1, 2] or equivalently by the semiclassical spectral determinant [25]. This belief is confirmed by studies of the Fourier transform of the (smoothed) quantum spectrum, which agrees reasonably well with periodic orbit predictions [21, 22, 23]. The semiclassical expression for the determinant, valid for systems with unstable, isolated periodic orbits only, has the form

$$D(E) = A(E)e^{-i\pi\overline{N}(E)} \exp\left(-\sum_p \sum_{r=1}^{\infty} \frac{\exp(irS_p(E)/\hbar - ir\alpha_p\pi/2)}{r\sqrt{|\det(\mathbf{1} - \mathbf{M}^r(E)_p)|}}\right). \tag{12}$$

The sum is taken here over all (single repeats of) periodic orbits of the system. The classical action $S_p = \oint p dq$ is taken along the periodic orbit, and $\mathbf{M}$ denotes the reduced Monodromy matrix, which describes the linearized dynamics in phase space perpendicular to the periodic orbit on the energy manifold. The Maslov index α counts twice the full rotations of the (real) eigenvectors of $\mathbf{M}$ around the orbit (plus two times the number of hard wall reflections). The

prefactors in front of the periodic orbit product are due to the zero-length limit in the Green function in a similar way as derived in (6), (8) and do not contribute to the spectrum. Eqn. (12) is formal in the sense, that it is not convergent for real energies [31] and suitable resummation techniques have to be applied [32, 24, 33, 34]. Thereby, the exponential function containing the periodic orbit sum is expanded and the resulting terms are regrouped by ordering them with respect to the total action or the total symbol length (after choosing a suitable symbolic dynamics). Such techniques have been shown to work successfully for hard chaos systems.

In the following, I will show that formula (12) is not valid for periodic orbits within a phase space region surrounding the bouncing ball family and will give explicit bounds for this area.

3.1 The Bogomolny Transfer Operator

Our starting point is the Bogomolny transfer operator [26] which is a semiclassical propagator for a classical Poincaré map. It has the form

$$T(q,q',E) = \frac{1}{(2\pi i\hbar)^{(f-1)/2}} \sum_{cl.tr q\to q'} \sqrt{\left|\frac{\partial^2 S}{\partial q \partial q'}\right|} e^{iS(q,q',E)/\hbar - i\nu\pi/2}, \tag{13}$$

where q, q' are points on an appropriate Poincaré surface of section in coordinate space and f denotes the number of degree of freedom. The sum has to be taken over all classical paths from q to q' crossing the Poincaré surface only once with momentum pointing in the direction of the normal to the surface. Again, $S(q,q';E)$ denotes the classical action along the path for fixed energy E. For billiard systems, it equals k times the length of the classical trajectory. The integer number ν counts the number of caustics in q–space (plus again twice the number of hard wall reflections). The semiclassical eigenvalues are given by the zeros of the determinant $\det(\mathbf{1}-\mathbf{T}(q,q',E))$. Evaluating the determinant in a cumulant expansion using the Plemelj–Smithies formula [26, 37]

$$\begin{aligned} \det(\mathbf{1}-\mathbf{T}) &= \sum_{n=0}^{\infty}(-1)^n \frac{\alpha_n(\mathbf{T})}{m!} \\ &= 1 - \mathrm{Tr}\mathbf{T} - \frac{1}{2}(\mathrm{Tr}\mathbf{T}^2 - (\mathrm{Tr}\mathbf{T})^2) - \dots \end{aligned} \tag{14}$$

with

$$\alpha_n(\mathbf{T}) = \begin{vmatrix} \mathrm{Tr}\mathbf{T} & n-1 & 0 & \dots & 0 \\ \mathrm{Tr}\mathbf{T^2} & \mathrm{Tr}\mathbf{T} & n-2 & \dots & 0 \\ \mathrm{Tr}\mathbf{T^3} & \mathrm{Tr}\mathbf{T^2} & \mathrm{Tr}\mathbf{T} & \dots & 0 \\ \vdots & \vdots & \vdots & \vdots & \vdots \\ \mathrm{Tr}\mathbf{T^n} & \mathrm{Tr}\mathbf{T^{n-1}} & \mathrm{Tr}\mathbf{T^{n-2}} & \dots & \mathrm{Tr}\mathbf{T} \end{vmatrix} \tag{15}$$

provides the connection to the expanded periodic orbit formula (12) using the iterates of the map as an expansion parameter. Periodic orbits appear as stationary phase points in the various traces and the amplitudes are recovered using the relation

$$\frac{1}{\sqrt{|\det(\mathbf{1}-\mathbf{M})|}} = \sqrt{\left|\frac{\partial^2 S(q,q')}{\partial q\partial q'}\Big|_{q=q'}\right|} \Big/ \sqrt{\left|\frac{\partial^2 S(q,q)}{\partial q^2}\right|}\,. \tag{16}$$

The stationary phase approximation demands periodic orbits to be unstable and sufficiently isolated. The last condition will be discussed in detail later. Note that the determinant and

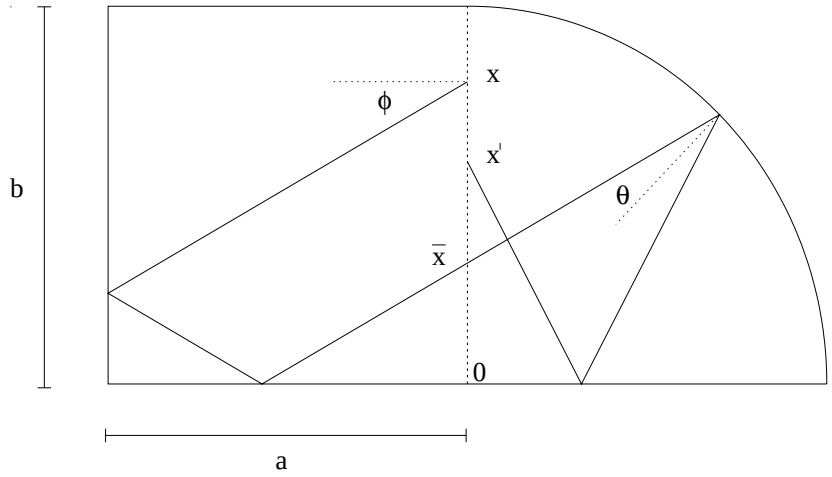

Figure 2: The quarter stadium billiard; the trajectory shown corresponds to $(m,l) = (-1,1)$.

the cumulant expansion (14) are well defined only if the operator $\mathbf{T}$ is *trace class*, which means essentially, that the trace of $\mathbf{T}$ exists and is finite in any basis. (For further details see [37], other expansion methods using Fredholm theory are discussed in [41]).

The Bogomolny transfer matrix method has been shown to work satisfactorily for hard chaos [42], mixed [42, 43] as well as integrable [38, 30, 42] systems, and has also been applied successfully to the stadium taking the billiard boundary as the Poincaré surface of section [30]. We seek now a Poincaré map which reflects the whole dynamics but excludes the bouncing ball orbits in order to obtain a semiclassical expression for the remainder D_r in (10). Choosing the intersection between the rectangle and the circle (the vertical dotted line in fig. 2) fulfills this criteria. The transfer operator corresponding to this Poincaré section takes on a particularly simple form for both the near bouncing ball limit and the whispering gallery limit. It is thus preferable to other possible choices such as e.g. the circle boundary.

3.2 The classical Poincaré Map

In the following, I will restrict attention to the stadium with $b = 1$. The spectrum for general b is obtained by simple scaling relations. I will consider the classical Poincaré map $(x, \phi) \to (x', \phi')$ with $x \in [0, 1]$ being the coordinate on the Poincaré plane starting from the bottom line. The angle $\phi \in]-\pi/2, \pi/2[$ corresponds to the momentum vector pointing away from the circle measured in the clockwise direction, see Fig. 2. (The corresponding energy dependent area preserving map is obtained in the coordinates $(x, p_x) = (x, \sqrt{2mE}\sin\phi)$.) The map can be written as

$$
\begin{aligned}
\overline{x} &= (-1)^m \left[x + 2a\tan\phi - (m + \frac{1-(-1)^m}{2}) \right] \qquad (17)\\
\overline{\phi} &= (-1)^m \phi \qquad \text{with} \quad m \le x + 2a\tan\phi < m+1 \\
\theta &= \arcsin(\overline{x}\cos\overline{\phi}) \\
\phi' &= \overline{\phi} + 2(l+1)\theta - k\pi \qquad \text{with} \quad l \le \frac{\overline{\phi}+\theta}{\pi - 2\theta} < l+1 \\
x' &= \overline{x}\,\frac{\cos\overline{\phi}}{\cos\phi'}.
\end{aligned}
$$

Figure 3: Members of the periodic orbit families approaching the bouncing ball orbits: a) (m, l) = (10, 0) and b) (m, l) = (-11, 1)

The coordinates $(\overline{x}, \overline{\phi})$ correspond to the first return at the Poincaré plane with momentum pointing toward the circle. The angle θ is the angle of incidence for reflections on the circular section of the boundary; see Fig. 2.

The length of a trajectory for one iteration of the map is

$$L(x,\phi) = \frac{2a + \cos(\overline{\phi} + \theta)}{\cos\phi} + 2l\cos\theta + \frac{\cos(\phi' - \theta)}{\cos\phi'}. \tag{18}$$

The general expression for the Monodromy matrix is given in Appendix A. The integer numbers $m \in [-\infty, \infty]$ correspond to $|m|$–reflections on the bottom or top line in the rectangle, the sign of m equals the sign of ϕ. The index $l \in [0, \infty]$ counts the number of free flights in the circle and corresponds to $(l + 1)$ – bounces with the circle boundary. The total number of bounces n_{tot} with the billiard boundary is thus

$$n_{tot} = |m| + (l + 1) + 2. \tag{19}$$

The map provides automatically a symbolic coding. It should be noted that the code does not form a "good" symbolic dynamics in the sense of Markov partition theory. Multiple iterates of the map are not uniquely encoded by symbol strings $\ldots, (m,l)_i, (m,l)_{i+1}, \ldots$, i.e. the partition is not generating. In addition, there is strong pruning, i.e. some of the possible symbols strings are not realized by trajectories of the map. The symbols defined by the map (17) do, however, reflect the important contributions of the dynamics to a semiclassical description as will be seen in the next section. The problem of finding a "good" symbolic dynamics for the stadium [39, 40] might be a consequence of this fundamental dilemma.

The bouncing ball limit $|m| \to \infty$ can be reached only for $l = 0$ or 1, but for all x on the Poincaré surface of section. The opposite limit $l \to \infty$, (the whispering gallery limit), is possible only for $m = 0$ or 1 and a decreasing x – interval of starting points. Together, there are four infinite series of fixed points of the map which are present for all parameter values a. In the $l = 0$ case, m must be even and positive. The corresponding periodic orbit family $(2n, 0)$, see Fig. 3a, has initial conditions

$$x_{(2n,0)} = 0, \quad \phi_{(2n,0)} = \arctan(n/a) \qquad \text{with} \quad n = 0, 1, \ldots \tag{20}$$

and

$$L_{(2n,0)} = \sqrt{(2n)^2 + (2a)^2} + 2, \qquad \det(\mathbf{1} - \mathbf{M}_{(2n,0)}) = 2L_{(2n,0)} - 4. \tag{21}$$

Note that $\det(\mathbf{1} - \mathbf{M})$ grows linearly with the length L and thus with the order parameter n which is in contrast to exponential growth for strictly hyperbolic dynamics.

The family with $l = 1$ approaching the bouncing ball orbits are formed by periodic orbits which start in a corner of the rectangle and bounce off perpendicular to the bottom line in the circle, see Fig. 3b. In this case, m must be odd and negative, i.e. $m = -2n - 1$. The angle of incidence θ for the bounce in the circle fulfills the condition

$$2\sin^2\theta + \frac{1}{a}(2n\cos\theta + 1)\sin\theta - 1 = 0, \quad n = 0, 1, \ldots \tag{22}$$

with approximate solution

$$\theta_n = \frac{a}{2n+1} + \mathcal{O}(n^{-3}).$$

The starting conditions on the Poincaré surface are

$$x_{(-2n-1,1)} = \frac{1}{2\cos\theta_n}, \quad \phi_{(-2n-1,1)} = -\frac{\pi}{2} + 2\theta_n < 0. \tag{23}$$

One obtains for the length of the periodic orbits

$$\begin{aligned} L_{(-2n-1,1)} &= 2\sqrt{(\cos\theta_n + n)^2 + (\sin\theta_n + a)^2} + 2\cos\theta_n & (24)\\ &= \sqrt{(2n)^2 + (2a)^2} + 4 - \frac{a^2}{2n^2} + \mathcal{O}(n^{-3}). & (25) \end{aligned}$$

and for the weight

$$\det(\mathbf{1} - \mathbf{M}_{(-2n-1,1)}) = 4\left(\frac{L_{(-2n-1,1)}}{\cos\theta_n} - 4\right) = 8n + 5\frac{a^2}{n} + \mathcal{O}(n^{-2}), \tag{26}$$

(see also appendix A). Again, the determinant increases linearly with the length of the periodic orbits.

An analysis of the periodic orbits $(0, l)$ and $(1, l)$ approaching the whispering gallery limit $l \to \infty$ is provided in appendix B.

3.3 The Poincaré map in the bouncing ball limit

The map (17) can be considerably simplified both in the bouncing ball limit and in the whispering gallery limit. The latter is postponed to appendix B.

For trajectories $(m, 0)$, one has to distinguish between four different cases: ($m \geq 0$, even), ($m < 0$, even), ($m > 0$, odd) and ($m < 0$, odd). One obtains for ($m \geq 0$, even)

$$\begin{aligned} x'_m &= \frac{\overline{x}}{1-2\overline{x}}\left[1 - \frac{4a^2}{d_m^2}\frac{\overline{x}(1-\overline{x})^2}{1-2\overline{x}}\right] + \mathcal{O}(m^{-4}) & (27)\\ \phi'_m &= \frac{\pi}{2} - \frac{2a}{d_m}(1-2\overline{x})\left[1 - \frac{4}{3}\frac{a^2}{d_m^2}\frac{1-\overline{x}(3-\overline{x}^2)}{1-2\overline{x}}\right] + \mathcal{O}(m^{-5}) & (28) \end{aligned}$$

with

$$d_m = 2a\tan\phi = m - x + \overline{x}.$$

The length of a trajectory is

$$L(x,\phi) = d + 2\frac{(1-\overline{x})^2}{1-2\overline{x}} + \frac{2a^2}{d_m} - \frac{4a^2}{d_m^2}\frac{\overline{x}^2(1-\overline{x})^2}{(1-2\overline{x})^2} - \frac{2a^4}{d_m^3} + \mathcal{O}(m^{-4}), \tag{29}$$

with $\overline{x}(x,\phi) = x + 2a\tan\phi - m > 0$. Note that x' depends at leading order on $\overline{x}$ only (and not independently on both x and ϕ). For the transfer operator (13), we need the length of a trajectory as function of the initial and final points x and x'. One obtains

$$\begin{aligned} L(x,x') &= m - x + x' + 2 + \frac{2a^2}{d_m}\left[1 - \frac{a^2}{d_m^2}\right] + \mathcal{O}(m^{-4}) && (30)\\ &= \sqrt{d_m^2 + (2a)^2} + x' - \frac{x'}{1+2x'} + 2 + \mathcal{O}(m^{-4}) \qquad x, x' \in [0,1] && (31)\\ \text{with} \qquad & d_m(x,x') = m - x + \frac{x'}{1+2x'}. && (32) \end{aligned}$$

The length of a trajectory after one iteration of the map is thus given by its length in the rectangle plus corrections which depend on x' only (up to $\mathcal{O}(m^{-4})$). The mixed second derivatives of $L(x,x')$ showing up in the transfer operator (13) are

$$\frac{\partial^2 L}{\partial x \partial x'} = -\frac{4a^2}{(d_m^2 + (2a)^2)^{3/2}(1+2x')^2} + \mathcal{O}(m^{-5}). \tag{33}$$

The length spectrum for the Poincaré map with m odd or negative is obtained by the following replacements in (30) – (33):

$(m<0$; even)	$m \to -m$	$x \to -x$	$x' \to -x'$	$x \in [0,1];\ x' \in [0,1/3]$
$(m>0$; odd)	$m \to m+1$		$x' \to -x'$	$x \in [0,1];\ x' \in [0,1/3]$
$(m<0$; odd)	$m \to -m-1$	$x \to -x$		$x \in [0,1];\ x' \in [0,1]$.

In a similar way, the approximate map for the $(m,1)$ – trajectories can be constructed. In the bouncing ball limit $m \to \infty$ only ($m \geq 0$, even) and ($m < 0$, odd) is possible. Again, we discuss first the case ($m \geq 0$, even), for which we obtain

$$\begin{aligned} x'_m &= \frac{\overline{x}}{4\overline{x}-1}\left[1 + \frac{8a^2}{d_m^2}\frac{\overline{x}}{4\overline{x}-1}(5\overline{x}^2 - 4\overline{x} + 1)\right] + \mathcal{O}(m^{-4}) && (34)\\ \phi'_m &= -\frac{\pi}{2} + \frac{2a}{d_m}(4\overline{x}-1)\left[1 - \frac{4}{3}\frac{a^2}{d_m^2}\frac{2\overline{x}(3-\overline{x}^2)-1}{4\overline{x}-1}\right] + \mathcal{O}(m^{-5}) && (35) \end{aligned}$$

with

$$d_m = m - x + \overline{x} = 2a\tan\phi.$$

The length of the trajectory as a function of the initial and final points is

$$\begin{aligned} L(x,x') &= m - x - x' + 4 + \frac{2a^2}{d_m}\left[1 - \frac{a^2}{d_m^2}\right] + \mathcal{O}(m^{-4}) && (36)\\ &= \sqrt{d_m^2 + (2a)^2} - x' - \frac{x'}{4x'-1} + 4 + \mathcal{O}(m^{-4}) && (37)\\ \text{with} \qquad & d_m(x,x') = m - x + \frac{x'}{4x'-1} \qquad x \in [0,1];\ x' \in [1/3,1] && (38)\\ \text{and} \qquad & \frac{\partial^2 L}{\partial x \partial x'} = -\frac{4a^2}{(d_m^2 + (2a)^2)^{3/2}(4x'-1)^2}. && (39) \end{aligned}$$

We recover the ($m < 0$, odd) case by replacing

$$(m<0;\text{odd}) \quad m \to -m-1 \quad x \to -x \qquad x \in [0,1];\ x' \in [1/3,1]$$

in (36) – (39).

3.4 The transfer operator T in the bouncing ball limit

The main advantage of a semiclassical description of quantum mechanics is to study directly the influence of (parts of) the classical dynamics on quantum phenomena. The importance of the near bouncing ball dynamics on the quantum spectrum can be understood by analyzing the T–operator obtained from the Poincaré map in the bouncing ball limit, see section 3.3.

The $\mathbf{T}$ –operator in the bouncing ball limit can be written as

$$T(x,x';k) = T_0(x,x',k) + \begin{cases} T_0(-x,-x',k) & \text{if} \quad 0 \le x' \le 1/3 \\ T_1(x,x',k) & \text{if} \quad 1/3 < x' \le 1 \end{cases} \tag{40}$$

with

$$\begin{aligned} T_0(x,x') &= 2a\sqrt{\frac{k}{2\pi i}}\frac{e^{ik(2+x'-\frac{x'}{1+2x'})-i\frac{3}{2}\pi}}{1+2x'}\sum_{n=0}^{\infty}\left[\frac{e^{ikL_0^-(n)}}{(L_0^-(n))^{3/2}} - \frac{e^{ikL_0^+(n)}}{(L_0^+(n))^{3/2}}\right] \\ T_1(x,x') &= -2a\sqrt{\frac{k}{2\pi i}}\frac{e^{ik(4-x'-\frac{x'}{4x'-1})-i\frac{3}{2}\pi}}{4x'-1}\sum_{n=0}^{\infty}\left[\frac{e^{ikL_1^-(n)}}{(L_1^-(n))^{3/2}} - \frac{e^{ikL_1^+(n)}}{(L_1^+(n))^{3/2}}\right] \end{aligned} \tag{41}$$

where $L_{0/1}^{\pm}(n)$ is defined as

$$L_0^{\pm}(x,x';n) = \sqrt{(2n \pm x + \frac{x'}{1+2x'})^2 + (2a)^2}; \tag{42}$$

$$L_1^{\pm}(x,x';n) = \sqrt{(2n \pm x + \frac{x'}{4x'-1})^2 + (2a)^2}. \tag{43}$$

Here, the lower index corresponds to $l = 0$ or 1. The upper index $-$ or $+$ distinguishes between contributions originating from trajectories with m even or odd. Note that trajectories in the bouncing ball limit have only one caustic in q–space inside the circle before returning to the Poincaré plane both for $l = 0$ and 1. The additional phases from hard wall reflections, see (19), have already been incorporated.

The operator (40) is the main result of this paper. It contains the dynamics in the stadium in a somewhat counterintuitive way. All contributions of trajectories with more than 2 reflections on the circle boundary are neglected. In addition, the short orbits for $l = 0$ or 1 are represented least accurately. This seems to contradict our common understanding of a semiclassical treatment of quantum mechanics for classically "chaotic" systems. The quantum spectrum for hard chaos systems is expected to be build up collectively by all unstable periodic orbits and the shortest periodic orbits are supposed to dominate an expansion of the spectral determinants (12) or (14). The stadium billiard posses, however, a subset of regular eigenstates, the so–called bouncing ball states, which show a nodal pattern very similar to the checkerboard pattern obtained for the unperturbed rectangular billiard. It is this subset of states which can be treated by the approximate transfer operator (40) alone. This is shown in Fig. 4. The leading terms in the cumulant expansion (14), i.e. $\det(\mathbf{1} - \mathbf{T}(k)) \approx 1 - \mathrm{Tr}\mathbf{T}(k)$, is plotted here as a function of k. The quantum eigenspectrum of the quarter stadium, marked by crosses on the k axis, is obtained from the boundary integral method. The eigenvalues having a bouncing ball nodal pattern are emphasized by arrows. (The bouncing ball states have been identified by inspecting individual wave functions). The minima of —$1 - \mathrm{Tr}\mathbf{T}(k)$— coincide very well with the eigenvalues corresponding to bouncing ball states found by our subjective criteria. The T–operator constructed from a Poincaré map in the bouncing ball limit fails in other regions of the spectrum. Some of the states are either completely ignored, see e.g. at $k \approx 7.6$, or they appear as

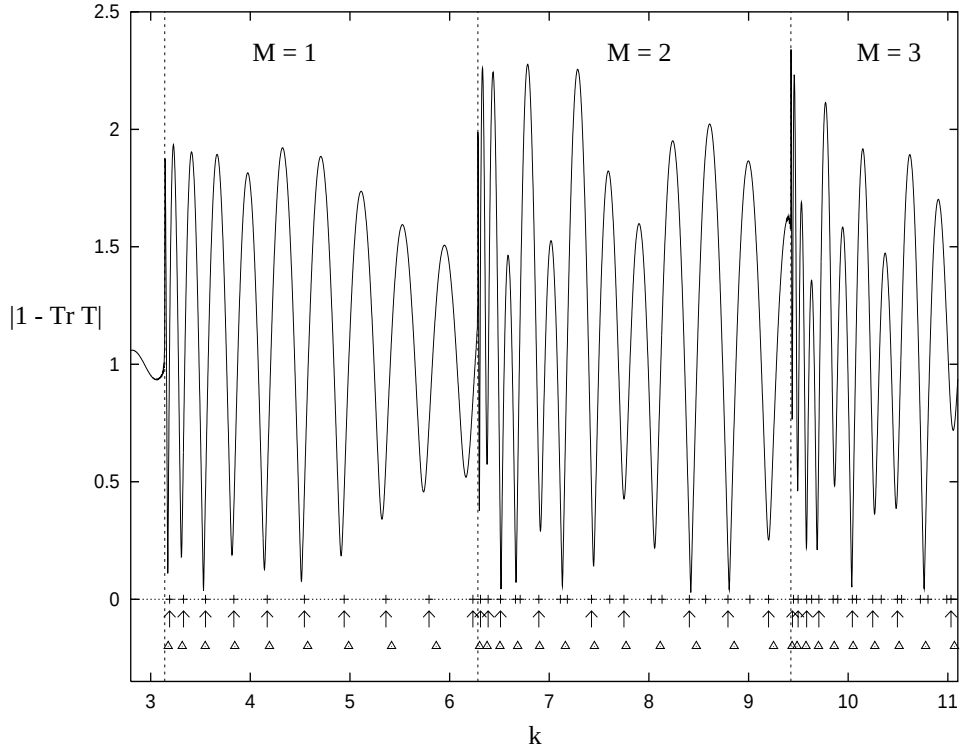

Figure 4: The absolute value of $1 - \mathrm{Tr}\mathbf{T}$ for $a = 5$ together with the quantum eigenvalues (+) and the quasi EBK – solutions ($\triangle$), see Eqn. (60) in section 3.6. The bouncing ball states are specially marked by arrows.

doublets, where the T – operator expects only a single state, see e.g. around $k \approx 6.7$. The latter case corresponds to a bouncing ball state interfering with a nearby state originating from the non–bouncing ball dynamics. By using higher terms in the cumulant expansion (or even the full determinant), non–bouncing ball behavior can partly be resolved. A quantization of the full spectrum cannot be expected, as important parts of the dynamics have been neglected. Note, that the trace of $\mathbf{T}$ has a cusp at $Rek = m\pi, m = 1, 2 \ldots$.

In the next section, the influence of periodic orbits which appear as stationary phase points in the trace of the T–operator will be studied in more detail.

3.5 The trace of T and periodic orbit contributions

Let us first concentrate on the trace of the $\mathbf{T}_0$ – part in the transfer operator (40) which contains contributions from trajectories with only one bounce on the circle boundary. The result for $\mathrm{Tr}\mathbf{T}_1$ will be given later. Expanding the length terms $L_0^{\pm}(n)$ up to $\mathcal{O}(n^{-2})$ in the exponent and to leading order in the amplitude, see (30), (33), yields

$$\begin{aligned} \mathrm{Tr}\mathbf{T}_0(k) &= \sum_{n=0}^{\infty} \mathrm{Tr}\mathbf{T}_{0,n}(k) \\ &= \frac{a}{2}\sqrt{\frac{k}{i\pi}} \sum_{n=0}^{\infty} \frac{1}{n^{3/2}} e^{ik(\sqrt{(2n)^2+(2a)^2}+2)-i\frac{3}{2}\pi} \end{aligned} \tag{44}$$

$$\int_{-1/3}^{1} \mathrm{d}x \frac{1}{1+2x} \left[\exp(ik\frac{a^2 \triangle^-}{2n^2}) - \exp(2ikx - ik\frac{a^2 \triangle^+}{2n^2}) \right].$$

with

$$\triangle^{\pm}(x) \;=\; x \pm \frac{x}{1+2x}.$$

The phases in front of the trace – integrals correspond to the length of the periodic orbits in the family $(m,l) = (2n,0)$, see (21). The negative region of integration comes form the second T_0 term in (40).

The dominant contribution to each integral is given by the first term containing $\triangle^-$ which derives from trajectories with an even number of reflections in the rectangle. It is stationary for $x = 0$, i.e. at the starting point of the periodic orbits (20). This becomes obvious after the change of variables,

$$\int_{-1/3}^{1} \mathrm{d}x \frac{1}{1+2x} \exp(ik\frac{a^2 \triangle^-}{2n^2}) = 2\int_0^{1/\sqrt{3}} dy \frac{1}{\sqrt{1+y^2}} \exp(ik\frac{a^2 y^2}{n^2}). \tag{45}$$

Approximating the integral straight forward by stationary phase, i.e. shifting the limits of integration to infinity, would lead to the standard periodic orbit amplitudes using (16), here for the periodic orbit family $(m,l) = (2n,0)$, see (21). The width of the Gaussian is, however, increasing with n and the finite limits of integration become important for $n \geq a\sqrt{k/\pi}$. The individual contributions to the sum (44) thus show a k–dependent transition, i.e.

$$\mathrm{Tr}\mathbf{T}_{0,n}(k) \;\to\; \frac{1}{2\sqrt{n}} e^{ik(\sqrt{(2n)^2+(2a)^2}+2)-i\frac{3\pi}{2}} \qquad \text{if} \quad n \ll a\sqrt{\frac{k}{\pi}} \tag{46}$$

$$\to\; \frac{a}{2}\sqrt{\frac{k}{\pi}} \frac{\log 3}{n^{3/2}} e^{ik(\sqrt{(2n)^2+(2a)^2}+2)-i\frac{7}{4}\pi} \qquad \text{if} \quad n \gg a\sqrt{\frac{k}{\pi}}. \tag{47}$$

Contributions from short trajectories in (46) have the Gutzwiller form for isolated unstable periodic orbits with amplitudes $|\det(\mathbf{1} - \mathbf{M}_n)|^{-1/2} \approx n^{-1/2}$ (see (21)) being independent of k. In the other limit $n \gg a\sqrt{\frac{k}{\pi}}$, we obtain $e^{ika^2y^2/n^2} \approx 1$ within the integration boundaries and the stationary phase approximation is no longer applicable. <u>All</u> trajectories in the range of integration give essentially the same contribution to the trace as the periodic orbit itself. A whole manifold of orbits build up the semiclassical weights in the trace in the same manner as manifolds of periodic orbits on tori with commensurable winding numbers do in a semiclassical treatment of integrable systems [4]. In our treatment as well as in the Berry–Tabor approach [4], the trace can be performed directly and no additional stationary phase approximation is needed (in contrast to the Gutzwiller formula). A comparison of (47) with the Berry–Tabor weights obtained for contributions in the rectangle, as e.g. in Eqn. (5), unveils the similarity. Note that the weights are now explicitly k–dependent and decrease like $n^{-3/2}$. The transition from "semiclassically integrable" to "chaotic" behavior affects mainly the amplitudes. The phase is in both cases essentially given by the length of the periodic orbit (21).

The conceptually different treatment for integrable and hard chaos systems can thus be rediscovered when studying intermittent dynamics near marginally stable boundaries. The contributions to the trace interpolate smoothly between the two extremes, the transition region itself is, however, $\hbar$ – (or k –) dependent. To the best of my knowledge, this has been shown here for the first time explicitly. The number of terms corresponding to contributions of isolated periodic orbits increases like $\sqrt{k}$, the turnover occurs for

$$n_0 \approx \log 3 \; a\sqrt{\frac{k}{\pi}}. \tag{48}$$

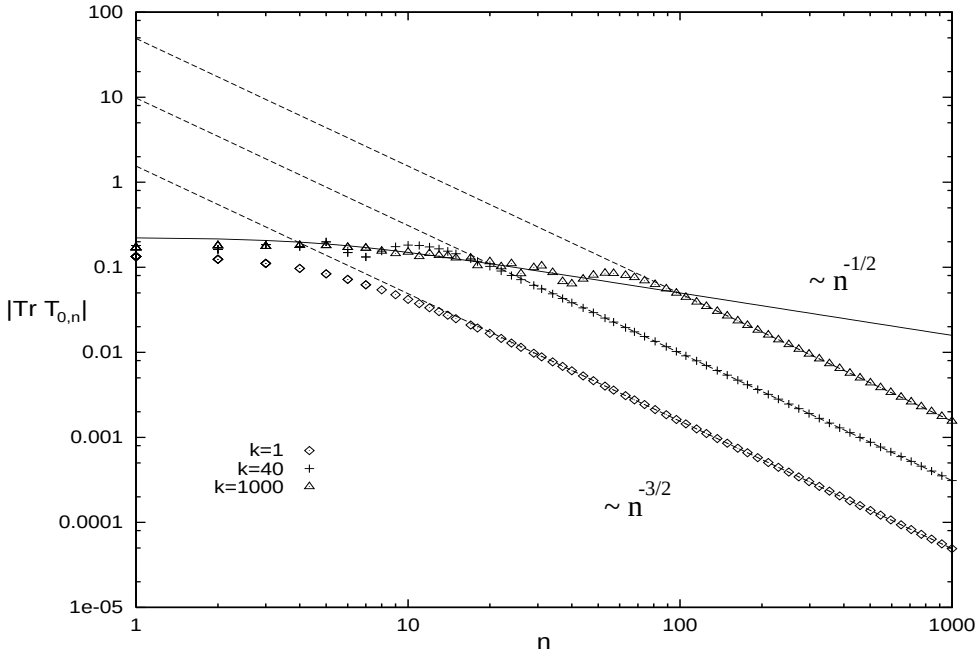

Figure 5: The modulus of $\mathrm{Tr}\mathbf{T}_{0,n}$ as function of the index n for different k–values showing a k–dependent transition from "chaotic" to "integrable" behavior with increasing n; the full line corresponds to $|\mathbf{1}-\mathbf{M}_n)|$, see (21), expected for isolated periodic orbits, the dashed lines is the k–dependent asymptotic form (47).

The transition is indeed rather sharp as can be seen in Fig. 5. The modulus of $\mathrm{Tr}\mathbf{T}_{0,n}$ is plotted here versus n for different k – values. The integral (44) has been calculated numerically using the full length formula (31). The oscillations occurring in the transition region correspond to the phase change from $3\pi/2$ to $7\pi/4$ from Eqs. (46) to (47).

The contributions to the trace from the second term in the integral (44) vanish like $1/\sqrt{k}$ for large k. They become, however, important for small k, especially for the k–region below the ground state.

In a similar way, the leading contributions to the $\mathbf{T}_1$ – operator in (40) (deriving now from the L_1^+ part, see (43) and thus from trajectories with $m<0$, odd) show a transition

$$\mathrm{Tr}\mathbf{T}_{1,n}(k) \;\rightarrow\; \frac{1}{2\sqrt{2n}}e^{ik(\sqrt{(2n)^2+(2a)^2}+4-\frac{a^2}{2n^2})} \qquad \text{if} \quad n \ll a\sqrt{\frac{k}{\pi}} \tag{49}$$

$$\rightarrow\; \frac{a}{4}\sqrt{\frac{k}{\pi}}\frac{\log 3}{n^{3/2}}e^{ik(\sqrt{(2n)^2+(2a)^2}+4-\frac{a^2}{2n^2})-i\frac{7}{4}\pi} \qquad \text{if} \quad n \gg a\sqrt{\frac{k}{\pi}}. \tag{50}$$

The phase is again essentially given by the lengths of periodic orbits from the family $(m,l) = ((-2n-1),1)$, see (25). A k–dependent transition occurs in the amplitude as in (46), (47) at a critical summation index approximately given by the estimate (48).

Our analysis suggests that a marginally stable boundary as provided here by the bouncing ball family is smoothly connected to the outer ergodic regions in a semiclassical treatment. We expect that this behavior is generic for systems with a mixed phase space structure. Stable islands are surrounded by a "semiclassically stable" layer and there is a smooth transition for semiclassical contributions from both sides of the classically disconnected regions. This effect has already been observed by Bohigas et al. [5, 44]. These authors compared the true quantum

spectrum in the quartic oscillator with an approximate EBK quantization of a stable island in this system. They were able to attach quantum states to EBK results even beyond the boundary given by the stable islands. This indicates an effective enlargement of the stable region into its "chaotic" neighborhood by quantum effects. Our analysis provides a consistent semiclassical interpretation of this phenomenon.

The results so far are based on the particular choice of the Poincaré surface of section. The approach presented here is opposite to a semiclassical quantization of the system on the billiard boundary. The trace of the transfer operator contains then only contributions from the shortest periodic orbits, especially from the marginal stable family. The Bogomolny method works for this section as well [30]. Note, however, that corrections to the Gutzwiller formula due to intermittency are introduced here through non–classical trajectories, when approximating the various traces by stationary phase. Note also that a naive summation using the Gutzwiller periodic orbit weights (46) for the stadium would give contributions of the form $\sum_{n=1}^{\infty} n^{-1/2} e^{ikL_n}$ which lead to true poles at $k = m\pi$. It is the $n^{-3/2}$ fall off for large n that prevents the trace as well as the spectral determinant from diverging at these points.

One might speculate why the corrections found here have not been observed in such a well–studied system like the stadium billiard. Previous studies were mainly based on Fourier transformation of the quantum spectrum. The Fourier transform exhibits peaks at positions corresponding to the length of periodic orbits. The Fourier spectrum is most sensitive to phases of semiclassical contributions and only the shortest periodic orbits are resolved when dealing with smoothed spectra or a finite energy interval. Intermittency as introduced through the bouncing ball family affects mainly the amplitudes and contributions of long trajectories. In addition, a k–dependence of the amplitudes as in (47), (50) is washed out by the Fourier integration. Fourier transformation is thus very insensitive to the influence of marginally stable behavior. In the next section, I will show that the bouncing ball spectrum indeed originates from series of orbits approaching the bouncing ball family and that there is no natural length cut–off for trajectories contributing dominantly to the transfer operator.

3.6 Discrete representation of the transfer operator and quasi EBK formulas

For a further analysis of the operator (40), we proceed in a very similar way to Ref. [38]. The infinite sums in (41) are convergent for $Im(k) \geq 0$ and may be expressed as

$$\sum_{n=0}^{\infty} \frac{e^{ikL_0^{\pm}(n)}}{(L_0^{\pm}(n))^{3/2}} = \frac{1}{2} \frac{e^{ikL_0^{\pm}(0)}}{(L_0^{\pm}(0))^{3/2}} + \sum_{m=-\infty}^{+\infty} \int_0^{\infty} \mathrm{d}n \frac{e^{ikL_0^{\pm}(n) - 2\pi i m n}}{(L_0^{\pm}(n))^{3/2}} \tag{51}$$

using Poisson summation [35]. The integral representation (51) provides an analytic continuation of the kernel (40) for $Im(k) < 0$ after rotating the axis of integration $\mathrm{d}n \to \pm i\,\mathrm{d}n$ [35, 36].

For k real, the integrals in (51) can be evaluated by stationary phase. The prefactors decrease not faster than algebraically and thus vary slowly compared to the phase. The stationary phase condition yields

$$k \frac{\partial L_0^{\pm}(n)}{\partial n} - 2\pi m = 0. \tag{52}$$

The solutions of (52),

$$n_m = \frac{1}{2} \left[\frac{2am}{\sqrt{k^2/\pi^2 - m^2}} \mp x - \frac{x'}{1 + 2x'} \right], \tag{53}$$

are real for $m \leq k/\pi$ only. The saddles for $m < 0$ give no contribution due to the limits of integration in (51). Note, that the sum is not necessarily dominated by short orbits. On the contrary, infinitely long trajectories give the main contributions to the sums in (41) when k approaches $m\pi$ from above. The singularities at $k = m\pi$ are linked to the cusps appearing in the bouncing ball contribution to the integrated trace (4) when summing over all repetitions of the marginal stable family.

By skipping the slowly varying first term on the LHS of (51), i.e. neglecting again short orbit contributions, one obtains in the stationary phase approximation

$$\begin{aligned} T_0(x,x') &\approx -i\frac{e^{2ki(1+\frac{x'^2}{1+2x'})+i\frac{\pi}{2}}}{1+2x'}\sum_{m=1}^{\infty} e^{2\pi i a\sqrt{k^2/\pi^2-m^2}}e^{i\frac{m\pi x'}{1+2x'}}\sin(m\pi x) \qquad (54)\\ T_1(x,x') &\approx i\frac{e^{4ki(1-\frac{x'^2}{4x'-1})+i\frac{\pi}{2}}}{4x'-1}\sum_{m=1}^{\infty} e^{2\pi i a\sqrt{k^2/\pi^2-m^2}}e^{i\frac{m\pi x'}{4x'-1}}\sin(m\pi x). \end{aligned}$$

The amplitudes are now no longer k–dependent. The sum over m disappears when writing the kernel (40) in the basis $\varphi_n = \sqrt{2}\sin(\pi n x), n = 1, 2, \ldots$, i.e.

$$T_{m,n} = \int_0^1 dx \int_0^1 dx' \varphi_m(x) T(x,x') \varphi_n(x'),$$

which leads to the discrete transfer matrix

$$T_{m,n}(k) \approx e^{2\pi i(a\sqrt{k^2/\pi^2-m^2}+\frac{k}{\pi}+\frac{1}{4})}\, R_{m,n}(k). \qquad (55)$$

The matrix $\mathbf{R}$ is given as

$$\begin{aligned} R_{m,n}(k) &= -i\int_{-1/3}^{1} dx' e^{2kix'^2/(1+2x')} e^{im\pi\frac{x'}{1+2x'}}\frac{\sin(n\pi x')}{1+2x'} \qquad (56)\\ &+ i\int_{1/3}^{1} dx' e^{2ik(1-2x'^2/(4x'-1))} e^{im\pi\frac{x'}{4x'-1}}\frac{\sin(n\pi x')}{4x'-1}, \end{aligned}$$

and is independent of the billiard length a. Applying the unitary transformation

$$\tilde{\mathbf{T}} = \mathbf{U}^{-1}\mathbf{T}\mathbf{U} \qquad \text{with} \quad U_{m,n} = e^{a\pi i\sqrt{k^2/\pi^2-n^2}}\delta_{n,m}\ , \qquad (57)$$

leads to the more symmetric form

$$\tilde{T}_{n,m}(k) \approx e^{2\pi i\left[\frac{a}{2}(\sqrt{k^2/\pi^2-n^2}+\sqrt{k^2/\pi^2-m^2})+\frac{k}{\pi}+\frac{1}{4}\right]}\, R_{n,m}(k). \qquad (58)$$

The transfer matrix (58) is now essentially finite with an effective dimension

$$\dim_{eff} = [k/\pi]\,, \qquad (59)$$

where the brackets [ ] denote the integer part of k/π. Formula (59) corresponds exactly to the estimate for the dimension of the T–operator given by Bogomolny [26] for the Poincaré surface chosen here. Neither the dimension nor the matrix $\mathbf{R}$ in (56) depend on the billiard parameter a which enters only through the phase in (55), (58). The T–operator derived from the Poincaré map in the bouncing ball limit is expected to reproduce best the bouncing ball states. The determinant can be approximated by its leading term in the cumulant expansion (14), i.e. $\det(\mathbf{1}-\mathbf{T}) \approx 1 - \mathrm{Tr}\mathbf{T}$. The phases in front of the matrix $\mathbf{R}$ in (58) yield a quantization condition for the bouncing ball spectrum. The matrix $\mathbf{R}$ acts as a filter determining the k – intervals, which allow for bouncing ball states in principle. A closer analysis shows that the

diagonal elements R_{mm} are dominant and approximately real in the region $k \in [m\pi, (m+1)\pi]$. This leads to an EBK–like quantization condition

$$a\sqrt{\frac{k^2}{\pi^2} - M^2} + \frac{k}{\pi} + \frac{1}{4} = M + N \qquad \text{for} \qquad \begin{aligned} M &= 1, 2, \ldots \\ N &= 1, 2, \ldots, [a\sqrt{2M+1} + 5/4]. \end{aligned} \tag{60}$$

M and N act as approximate quantum numbers corresponding to bouncing ball eigenfunctions with $(M-1)$ nodal lines perpendicular and $(N-1)$ nodes parallel to the Poincaré surface. (An additional M on the RHS of (60) is introduced for convenience). The cut–off in the N – quantum number originates from the k–window given by the $\mathbf{R}$ matrix. The states with fixed quantum number M are restricted to the interval $k \in [M\pi, (M+1)\pi]$ and different M series do not overlap.

In table 1, the bouncing ball eigenvalues (chosen by inspection of at the individual wavefunctions) are compared with the quasi EBK quantization condition (60) for $a = 5$. The EBK – solutions are also marked in Fig. 4. The importance of the additional terms $k/\pi + 1/4$ becomes evident when comparing the results with the spectrum of the rectangle obtained from to the condition $a\sqrt{k^2/\pi^2 - M^2} = N$, i.e. $k^2/\pi^2 = M^2 + N^2/a^2$. Again, we find that some bouncing ball states expected from the EBK formula (60) appear to have lost their regular nodal pattern due to interference with non–bouncing ball states.

Note, that the T–operator for the rectangle [38] is not recovered in the limit $a \to \infty$. The $\mathbf{R}$ matrix (56) is independent of a and the circle boundary can thus not be treated as a small perturbation even for large a values. The solutions of (60) can approximately be written in the form

$$\begin{aligned} \frac{k_{M,N}^2}{\pi^2} &= M^2 + \frac{1}{a^2}(N - \Delta_{N,M} - \frac{1}{4})^2 \\ \text{with} \qquad \Delta_{N,M} &= \sqrt{M^2 + \left(\frac{N - 1/4}{a}\right)^2} - M \to 0 \quad \text{for} \quad M \gg \frac{N}{a}. \end{aligned} \tag{61}$$

A rectangular–like spectrum is achieved in the "integrable" limit $a \to \infty$, however, in a very special way. First of all, Eqn. (61) contains an extra phase 1/4 originating from the caustic in the circle, which is not present in the rectangle. In addition, the different M–series always have a finite cut–off for finite a, see (60). The number of states in a given M series increases to infinity only in the limit $a \to \infty$.

The determinant $\det(\mathbf{1} - \mathbf{T})$ is analytic in each strip $Rek \in]m\pi, (m+1)\pi[$, with m integer, but has a cusp at $k = m\pi$. The non–analytic behavior is introduced through infinitely long trajectories contributing in leading order at $k\pi \approx m$, see Eqn. (53). These cusps are a consequence of omitting the bouncing ball contributions, which itself exhibit a cusp at integer multiples of π, see Eqn. (4). The full spectral determinant $D(k)$ (10) is analytic and nonanalytic behavior in the bouncing ball contributions is canceled by the near–bouncing ball dynamics.

Of special interest is, however, the maximal length of trajectories necessary to resolve the regular part of the quantum spectrum at a given wave number k. Inserting (61) in (53) leads to an estimate for the trajectory lengths contributing dominantly to the ground state $(M, N = 1)$ in each M series, i.e. to the state located next to the cusp $k = M\pi$. We obtain

$$L_{max} \approx n_{max} \approx \frac{4}{3}a^2 M \approx \frac{4}{3}a^2\frac{k}{\pi}. \tag{62}$$

	k_{qm}	k_{ebk}	k_{qm}	k_{ebk}	k_{qm}	k_{ebk}
M	1		2		3	
N=1	3.190 (1)	3.176	6.309 (11)	6.301	9.441 (29)	9.436
2	3.329 (2)	3.317	6.386 (12)	6.375	9.497 (31)	9.487
3	3.550 (3)	3.547	6.510 (13)	6.505	9.583 (32)	9.576
4	3.835 (4)	3.844		6.683	9.706 (34)	9.701
5	4.170 (5)	4.191	6.896 (16)	6.904		9.860
6	4.542 (6)	4.575		7.162	10.042 (37)	10.049
7	4.942 (7)	4.986	7.423 (19)	7.452	10.245 (39)	10.267
8	5.361 (8)	5.418	7.750 (21)	7.771	10.494 (41)	10.511
9	5.793 (9)	5.865		8.113		10.777
10	6.233 (10)	6.325	8.405 (24)	8.475	11.032 (44)	11.065
11			8.793 (26)	8.855	11.350 (48)	11.373
12			9.201 (28)	9.251		11.697
13					11.982 (53)	12.038

Table 1: Eigenvalues k_{qm} belonging to bouncing ball eigenstates compared with the EBK-like quantization condition (60) for $a = 5$; here, N, M denote the approximate quantum numbers; the numbers in brackets correspond to an enumeration of all states in successive order.

This is in contrast to general semiclassical arguments for bound systems leading to a cut–off for periodic orbits sums at half the Heisenberg time [24]. This transforms for billiard into a cut–off in the length spectrum according to

$$L_{max} = \pi \overline{d}(k) \approx \frac{A}{4} k, \tag{63}$$

where $\overline{d}(k)$ is the mean level density and A the area of the billiard. The estimate (62) scales differently with the billiard parameter a and deviates thus especially in the "integrable" limit $a \to \infty$. The cut–off (63) as derived in Ref. [24] is based on two main assumptions: the overall validity of the Gutzwiller periodic orbit formula and the analyticity of the semiclassical spectral determinant in a strip containing the real energy axis. Both assumptions which might be intimately related for bound systems fail here. Note, that this is not necessarily true for scattering systems. A semiclassical quantization of two examples showing intermittency, the Helium atom [35] and Hydrogen in a constant magnetic field for positive energy [36], could be achieved within the Gutzwiller approach. However, the intermittent part of the dynamics introduces in these cases as well regular structures in the resonance spectrum and non–analyticity in the spectral determinant.

4 The bouncing ball states

The threshold (48) can be interpreted as the boundary of a region in phase space surrounding the marginal stable bouncing ball family. Semiclassical contributions from the dynamics in this region have a form similar to the one obtained for stable islands [5, 6] or in integrable systems [3, 4]. The threshold values can be directly translated into momenta in phase space, i.e. $p_x^t = \pm k \sin\phi_t$ with $\phi_t \approx \arctan(n_{0,1}/a) \approx \arctan\sqrt{k/\pi}$, see Eqn. (17). A *semiclassically stable*

island can thus be defined covering a phase space volume $V_{reg} = k^2 \tilde{V}_{reg}$ with

$$\begin{aligned} \tilde{V}_{reg}(k) &= 4a \int_{\phi_t}^{\pi/2} \mathrm{d}\phi \approx 4a \left(\frac{\pi}{2} - \arctan \sqrt{\frac{k}{\pi}} \right) \\ &\approx 4a\sqrt{\frac{\pi}{k}} \qquad \text{for} \quad k/\pi \gg 1. \end{aligned} \tag{64}$$

The size of the semiclassical island approaches zero in the limit $k \to \infty$ (compared to the volume of the full phase space). The number of quantum states associated with this island thus increases like

$$\overline{N}_{reg}(k) \approx a \left(\frac{k}{\pi} \right)^{3/2} + \mathcal{O}(\sqrt{k/\pi}). \tag{65}$$

on average. This estimate coincides with the average increase of regular states given by the EBK–quantization condition (60). It exceeds previous results by O'Connor and Heller [46], who obtained a linear increase in k for the number of localized bouncing ball states up to the semiclassical limit $k \to \infty$. Note, that a $k^{3/2}$ increase in the number of bouncing ball states is still consistent with the Schnirelman theorem [47], as the fraction of regular states compared to all eigenstates approaches zero in the semiclassical limit.

The oscillating part of the level staircase function

$$N_{osc}(k) = N(k) - \overline{N}(k) \tag{66}$$

shows a strong periodic modulation in the stadium, see Fig. 6a. ($N(k) = \sum_n \theta(k - k_n)$ denotes here the quantum level staircase function and $\overline{N}$ its mean part given by the Weyl formula [45]).

This modulation coincides with the oscillating part of the bouncing ball contributions [21, 22, 23], see Eqn. (4). It was shown in section 2, that the bouncing ball family does not contribute to individual eigenvalues. From the point of view of individual states in the spectrum, the oscillatory behavior in the level staircase function is caused by a periodic change in the spacings between neighboring eigenvalues. The spacings are unaffected by contributions coming from the classical bouncing ball family.

Taking the concept of a semiclassical stable island seriously, we expect the spectrum of the stadium billiard to be divided into two different subspectra. The majority of states belong to the "chaotic" subspace formed by non–localized eigenstates (leaving aside the phenomenon of scaring along short unstable trajectories). Their number increases on average like

$$\overline{N}_{chaos}(k) = \overline{N}(k) - \overline{N}_{reg}(k) \approx \frac{A}{2\pi} k^2 - a \left(\frac{k}{\pi} \right)^{3/2} + \mathcal{O}(k), \tag{67}$$

and the volume of the billiard is $A = a + \pi/4$. The level statistics of this subspectrum is expected to follow the GOE prediction of random matrix theory. The statistics as well as the average level repulsion is then stationary, i.e. independent of k, in the unfolded spectrum. The level staircase function is expected to be structureless showing only "statistical" fluctuations around the mean value $\overline{N}_{chaos}(k)$. The regular subspectrum contains the eigenstates originating from a quantization of the bouncing ball island (64). The coupling of the dynamics in the "semiclassically integrable" region to the outer classical motion is weak compared to the mixing in the outer region itself. The level repulsion between bouncing ball states and chaotic eigenstates is thus small compared to the coupling among non–bouncing ball states itself. A possible structure in the level staircase function for the regular states which can be obtained from the EBK– quantization condition (60) can therefore survive in the full spectrum. This is indeed the

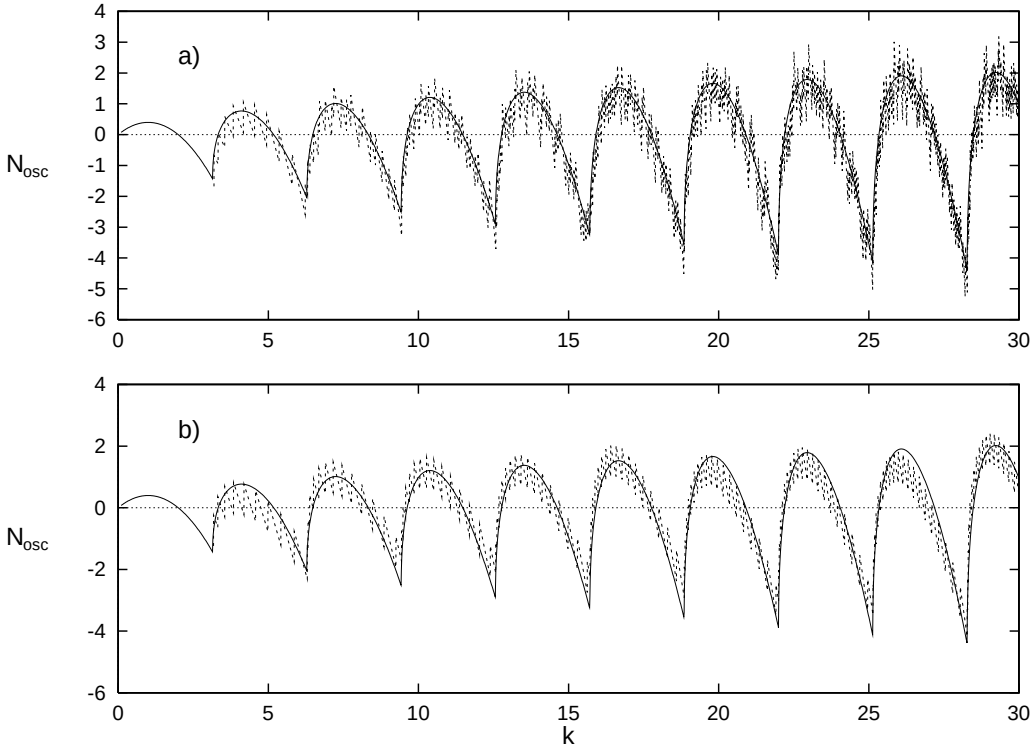

Figure 6: The oscillating part of the level staircase function (a) for the full spectrum; (b) for the bouncing ball states only. The full line corresponds to the oscillating part of the bouncing ball contributions, see (4).

case. The oscillating part of the EBK – level staircase function can be defined with the help of Eqn. (65), i.e.

$$N_{osc}^{reg}(k) = N_{EBK}(k) - \overline{N}_{reg}(k). \tag{68}$$

Here, $N_{EBK}(k)$ is given by the number of levels obtained from the quantization condition (60) up to a certain k – value. The result is shown in Fig. 6b, (where the next to leading terms in $\overline{N}_{reg}$ have been fitted numerically). The function N_{osc}^{reg} shows exactly the same modulations as the full spectrum and coincides also with the oscillating part of the bouncing ball contributions. We conclude, that *the dominant oscillation in the level staircase function of the full spectrum is caused by a modulation in the density of bouncing ball states only.*

5 Conclusion

I have shown that the marginally stable bouncing ball family in the stadium billiard does not contribute to individual quantum eigenvalues. The result is confirmed by a semiclassical quantization of the quarter stadium using Bogomolny's transfer matrix technique in a representation which excludes the bouncing ball orbits explicitly. The regular bouncing ball quantum states in the spectrum derive semiclassically from the near bouncing ball dynamics alone, and these states follow a simple quantization rule. The trace of the transfer operator can be approximated by periodic orbit contributions, which, however, show a $\hbar$–dependent transition from Gutzwiller to Berry–Tabor–like behavior when approaching the bouncing ball family. This leads to the concept of a semiclassical island of stability surrounding the marginal stable family in phase

space. The boundary of this region is explicitly $\hbar$–dependent and the phase space volume of the island shrinks to zero (compared to the total volume) in the semiclassical limes $\hbar \to 0$ (or $k \to \infty$). The quasi EBK – quantization formula can be associated with a quantization of the semiclassical stable island. The periodic modulations in the level staircase function can be related to a periodic change in the density of bouncing ball eigenstates.

The results demonstrate that averaged dynamical properties like ergodicity and positive Liapunov exponent are not sufficient to ensure the applicability of the Gutzwiller trace formula. The "chaoticity" of the stadium is in a semiclassical sense indeed $\hbar$–dependent, and the billiard is for small k closer to an integrable system than to a hard chaos one.

The Gutzwiller periodic orbit weights have to be modified in the whispering gallery limit as well, see appendix B. An accumulation of periodic orbits towards a limiting cycle of finite length has also been found in other systems as e.g. in the cardioid billiard [49, 48], in the wedge billiard [40, 42] and in the Anisotropic Kepler Problem [1, 50]. We expect that a careful treatment as outlined in the appendix will solve problems concerning a semiclassical quantization of these systems.

The results obtained here for the stadium billiard are expected to be generic for systems with mixed phase space structure (however complicated by the existence of island chains and can–tori surrounding the stable island itself). The stable island influences the classical dynamics in the outer chaotic region by creating intermittency. The regular regions appear to be larger than the actual size of the stable island due to the finite phase space resolution of quantum mechanics. The findings explain in a natural way the existence of EBK quantum states associated with regions outside a stable island as found in [5, 44]. The width of this semiclassically integrable layer is $\hbar$ dependent. A semiclassical quantization of stable islands as well as the behavior of localized wave functions on classical boundaries and the description of tunneling through dynamical separatrices [5, 12, 13] will be sensitive to this behavior. The results derived here indicate a failure of the Berry–Keating periodic orbit resummation [24] for mixed systems due to the intermittency introduced by the stable regions.

The work presented here is restricted to semiclassical aspects. The influence of intermittency on Frobenius–Perron and related classical operators [51, 52] is so far best described by a so called BER–approximation [53]. The spectra of classical operators are directly related to classical [54, 55] and semiclassical sum rules [56] as well as to spectral statistics [56, 57, 58] in hard chaos systems. The influence of intermittency on these results is still an open issue.

Remark:
When completing this article, I became aware of a recent work carried out by Primack et. al. [59]. The authors discus diffraction in the Sinai billiard by analyzing the Fourier transformation of the true quantum spectrum in detail. They could indeed relate all deviations from the Gutzwiller trace formula to diffraction effects (due to the concave boundaries in this billiard) except for some of the near bouncing ball orbits. The results in [59] indicate clearly, that the influence of intermittency as dicussed in this article can also be seen directly in the Fourier spectrum.

Acknowledgment:

I would like to thank Debabrata Biswas, Predrag Cvitanović, Bertrand Georgeot, Kai Hansen, Jon Keating and Mark Oxborrow for stimulating discussions and useful comments on the manuscript. The work was supported by the Deutsche Forschungsgemeinschaft.

A Monodromy matrix in the stadium billiard

The Monodromy matrix used in section 3 describes the linearized motion near a classical trajectory in phase space in a plane perpendicular to the orbit and on the energy manifold. For billiard systems, this plane is spanned by the local displacement vectors $\delta q_\perp$, $\delta p_\perp$ pointing perpendicular to the actual momentum of the trajectory. An initial displacement is thus propagated according to

$$\begin{pmatrix} \delta q_\perp^t \\ \delta p_\perp^t \end{pmatrix} = \mathbf{M}_{q(t),p(t)} \begin{pmatrix} \delta q_\perp^0 \\ \delta p_\perp^0 \end{pmatrix},$$

where $\mathbf{M}$ depends on the path of the underlying trajectory. For 2–dimensional billiards, one obtains

$$\mathbf{M}(t) = \begin{pmatrix} 1 & L/k \\ 0 & 1 \end{pmatrix},$$

where $t = L/k$ denotes the time between two bounces at the boundary, L is the length of the path and $k = \sqrt{2mE}$. The contribution from a reflection at the boundary is

$$\mathbf{M}_r = \begin{pmatrix} -1 & 0 \\ \frac{2k\kappa}{\cos\theta} & -1 \end{pmatrix},$$

where κ denotes the local curvature of the boundary, and θ is the angle between the orbit and the normal to the boundary. The k – dependence is scale invariant due to the transformation $\delta q(k) = \delta q(k=1)$, $\delta p(k) = k\delta p(k=1)$ and we may set $k = 1$ in what follows.

Bounces on straight lines in the stadium billiard are treated as free flights. The angle of incidence θ is the same for all successive bounces of an orbit in the circle. The length between two of these bounces is $L = 2b\cos\theta$ where b denotes the radius of the circle. The Monodromy matrix for l free flights in the circle interrupted by $(l+1)$ successive reflections on the circle boundary is thus given by

$$\mathbf{M} = \begin{pmatrix} -(1+2l) & 2lb\cos\theta \\ \frac{2(l+1)}{b\cos\theta} & -(1+2l) \end{pmatrix}. \tag{69}$$

B The whispering gallery limit

The whispering gallery limit of the Poincaré map (17) is formed by trajectories (m, l) with m fixed and $l \to \infty$ in the notation of section 3.2. These orbits approach the boundary of the billiard with an increasing number of bounces in the circle. Only $m = 0$ and $m = 1$ is possible in the limit $l \to \infty$. I will consider here the case $m = 0$ and $b = 1$. The approximate whispering gallery map for $m = 1$ follows by analogy.

There is one fixed point for each symbol pair $(m = 0, l)$ with starting conditions

$$x_l = \cos\left(\frac{\pi}{2}\frac{1}{l+1}\right); \quad \phi_l = 0. \tag{70}$$

The angle of incidence θ for reflections in the circle is

$$\theta_l = \frac{l}{l+1}\frac{\pi}{2}. \tag{71}$$

The length of the corresponding periodic orbit approaches a constant, i.e.

$$L_l = 2a + 2(l+1)\cos\theta_l = 2a + \pi - \frac{\pi^3}{24}\frac{1}{(l+1)^2} + \mathcal{O}(l^{-4}). \tag{72}$$

The Monodromy matrix along the orbits starting on the Poincaré surface of section can be deduced from appendix A and is

$$\mathbf{M}_l = \begin{pmatrix} 1 & 2a \\ \frac{2(l+1)}{\cos\theta_l} & \frac{4a(l+1)}{\cos\theta_l} + 1 \end{pmatrix}. \tag{73}$$

The periodic orbit weighting factor $|\det(\mathbf{1} - \mathbf{M}_l)|$ is thus

$$|\det(\mathbf{1} - \mathbf{M}_l)| = 4a\frac{l+1}{\cos\theta_l} = \frac{8a}{\pi}(l+1)^2 + \frac{\pi}{3}a + \mathcal{O}(l^{-2}). \tag{74}$$

The determinant and thus the largest eigenvalue Λ_l of the Monodromy matrix increase quadratically with the symbol index. The main difference compared to the bouncing ball limit is the convergence of the period L_l towards a finite value: the length of the billiard boundary. The whispering gallery limit therefore introduces no intermittency. The Liapunov – exponent of periodic orbits,

$$\lambda_l = \frac{\log\Lambda_l}{L_l} \sim \log l,$$

diverges logarithmically and the boundary orbit $(0, l = \infty)$ is infinitely unstable.

I will show below that the isolated orbit condition is again violated when taking the trace of the transfer operator. A naive summation of Gutzwiller periodic orbit weights would overestimate the whispering gallery contributions considerably. The breakdown of the stationary phase condition is caused here by the accumulation of periodic orbits, i.e. stationary phase points, near the billiard boundary.

The phase space area of starting conditions on the Poincaré surface for trajectories with the same l–value is centered on the corresponding periodic orbit. Its size shrinks to zero in the limit $l \to \infty$ both in the x and ϕ coordinate. The transfer operator in the whispering gallery limit is thus directly given by the Jacobian matrix (73) in local coordinates $\delta x = x - x_l$, $\delta\phi = \phi - \phi_l$ centered on the fixed points (70). The orbit length is approximately given by the quadratic form

$$L_l(\delta x, \delta x') = L_l + \frac{1}{2}\begin{pmatrix} \delta x \\ \delta x' \end{pmatrix}^T \mathbf{J}_l \begin{pmatrix} \delta x \\ \delta x' \end{pmatrix}$$

with

$$\mathbf{J}_l = \begin{pmatrix} \frac{\partial^2 L}{\partial x \partial x} & \frac{\partial^2 L}{\partial x \partial x'} \\ \frac{\partial^2 L}{\partial x' \partial x} & \frac{\partial^2 L}{\partial x' \partial x'} \end{pmatrix}_{x=x'=x_l} = \begin{pmatrix} \frac{1}{2a} & -\frac{1}{2a} \\ -\frac{1}{2a} & \frac{1}{2a} + \frac{2(l+1)}{\cos\theta_l} \end{pmatrix},$$

where L_l denotes the length of the periodic orbit. When taking the trace of $\mathbf{T}$ we are interested in trajectories satisfying $\delta x = \delta x'$ which demands $\delta\phi = 0$. More important is, however, the restrictions on the δx – interval, i.e.

$$-\frac{\pi}{2}\frac{\cos\theta_l}{(l+1)(2l+1)} \le \delta x < \frac{\pi}{2}\frac{\cos\theta_l}{(2l+3)(2l+1)}. \tag{75}$$

The interval length and thus the integration range decreases like l^{-3}.

The whispering gallery contribution to the trace of the $\mathbf{T}$ – operator are

$$\mathrm{Tr}\mathbf{T}_{wg} = \sum_{l=0}^{\infty} \frac{1}{\sqrt{2\pi i}} \sqrt{\frac{k}{2a}} e^{ikL_l - i\frac{3}{2}(l+1)\pi} \; 2\int_0^{\overline{\delta}} \mathrm{d}x \, e^{ik\frac{l+1}{\cos\theta_l}x^2}, \tag{76}$$

where the upper and lower limits in (75) have been approximated by their mean value

$$\overline{\delta} = \pi \frac{\cos\theta_l}{(2l+1)(2l+3)} \approx \frac{\pi^2}{2} \frac{1}{(l+1)(2l+1)(2l+3)}.$$

The interval length decreases faster than (the square root of) the prefactor in the exponent for increasing l. A stationary phase approximation is not justified for $l \to \infty$, and we obtain (as in the bouncing ball limit) a transition behavior

$$\mathrm{Tr}\mathbf{T}_{wg}^{l} \;\; \to \;\; \frac{1}{\sqrt{|\det(\mathbf{1}-\mathbf{M_l}|}} e^{ikL_l - i\frac{3}{2}(l+1)\pi} \qquad \text{for} \quad l \ll \left(\frac{\pi}{2}k\right)^{1/4} \tag{77}$$

$$\mathrm{Tr}\mathbf{T}_{wg}^{l} \;\; \to \;\; \sqrt{\frac{\pi k}{a}} \frac{\cos\theta_l}{(2l+1)(2l+3)} e^{ikL_l - i\frac{3}{2}(l+1)\pi - i\frac{\pi}{4}} \qquad \text{for} \quad l \gg \left(\frac{\pi}{2}k\right)^{1/4}. \tag{78}$$

Note, that the number of periodic orbits which can be treated as isolated stationary phase points, increases only at a rate proportional to $k^{-1/4}$. The contributions for large l fall off like l^{-3} and thus faster than in the bouncing ball case. In addition, there is a cancelation between the $(0,l)$ and the $(1,l)$ family which show the same overall behavior but appear with opposite signs. The whispering gallery contributions are thus small compared to near bouncing ball contributions, at least for $a \geq 1$.

References

[1] M. C. Gutzwiller, *Chaos in Classical and Quantum Mechanics* (Springer, New York, 1990).

[2] R. Balian and C. Bloch, Ann. Pays. (N.Y.) **69**, 75 (1972); **85**, 514 (1974).

[3] M. V. Berry and M. Tabor, Proc. Roy. Soc. London A **349**, 101 (1976).

[4] M. V. Berry and M. Tabor, J. Phys A **10**, 371 (1977).

[5] O. Bohigas, S. Tomsovic and D. Ullmo, Phys. Rep. **223**, 44 (1993).

[6] D. Wintgen and K. Richter, Comm. At. Mol. Phys. **29**, 261 (1994).

[7] A. M. Ozorio de Almeida and J. H. Hannay, J. Phys. A **20**, 5873 (1987).

[8] S. Tomsovic, M. Grinberg and D. Ullmo, Phys. Rev. Lett. **75**, 4346 (1995).

[9] K. Richter, D. Ulmo and R. Jalabert Phys. Rep. (in press); K. Richter, D. Ulmo and R. Jalabert, *Disorder Effects in Ballistic Microstructures*, submitted to Phys. Rev. B (1996).

[10] M. Sieber, J. Phys. A, **29**, 4715 (1996).

[11] S. C. Creagh, Ann. Phys. **248**, 60 (1996). preprint (1996).

[12] A. Shudo and K. S. Ikeda, Phys. Rev. Lett. **74**, 682 (1995).

[13] E. Doron and S. D. Frischat, Phys. Rev. Lett. **75**, 3661 (1995).

[14] H. G. Schuster, *Deterministic Chaos* (VCH, Weinheim, 1989).

[15] L. A. Bunimovich, Comm. Math. Phys. **65**, 295 (1979); see also L. A. Bunimovich Chaos **1**, 187 (1991).

[16] S. W. McDonald and A. K. Kaufman, Phys. Rev. Lett. **42**, 1189 (1979); Phys. Rev. A **37**, 3067 (1988).

[17] G. Casati and F. Valz–Gris, and I. Guarnieri, Lett. Nuovo Cimento **28**, 279 (1980).

[18] O. Bohigas, M. J. Giannoni and C. Schmit, Phys. Rev. Lett. **52**, 1 (1984).

[19] E. J. Heller, Phys. Rev. Lett. **53**, 1515 (1984).

[20] H.-J. Stöckmann and J. Stein, Phys. Rev. Lett. **64**, 2215 (1990); **68**, 2867 (1992).

[21] H.–D. Gräf, H. L. Harney, H. Lengeler, C. H. Lewenkopf, C. Rangacharyulu, A. Richter, P. Schardt and H. Weidenmüller , Phys. Rev. Lett. **69**, 1296 (1992).

[22] M. Sieber, U. Smilansky, S. C. Creagh and R. G. Littlejohn, J. Phys. A **26**, 6217 (1993).

[23] D. Alonso and P. Gaspard, J. Phys. A **27**, 1599 (1994).

[24] M. V. Berry and J. P. Keating, J. Phys. A **23**, 4839 (1990); M. V. Berry and J. P. Keating, Proc. R. Soc. A **437** 151 (1992).

[25] A. Voros, J. Phys. A **21**, 685 (1988).

[26] E. B. Bogomolny, Nonlinearity **5**, 805 (1992).

[27] A, Voros, Commun. Math. Phys. **110**, 439 (1987).

[28] J. P. Keating and M. Sieber, Proc. R. Soc. A **447**, 413 (1994).

[29] J. P. Keating and M. V. Berry, J. Phys. A **20**, L1139 (1987).

[30] P. A. Boasman, Nonlinearity **7**, 485 (1994); Phd–thesis *Semiclassical Accuracy for Billiards*, University of Bristol (1992).

[31] B. Eckhardt und E. Aurell, Europhys. Lett. **9**, 509 (1989).

[32] P. Cvitanović, Phys. Rev. Lett. **61**, 2729 (1988); P. Cvitanović and B. Eckhardt, Phys. Rev. Lett. **63**, 823 (1989).

[33] G. Tanner, P. Scherer, E. Bogomolny, B. Eckhardt and D. Wintgen, Phys. Rev. Lett. **67**, 2410 (1991).

[34] M. Sieber and F. Steiner, Phys. Rev. Lett. **67**, 1941 (1991).

[35] G. Tanner and D. Wintgen, Phys. Rev. Lett. **75**, 2928 (1995).

[36] G. Tanner, K. T. Hansen and J. Main , *The semiclassical resonance spectrum of Hydrogen in a constant magnetic field*, to be published in Nonlinearity (1996).

[37] A. Wirzba and M. Henseler, unpublished, Darmstadt, 1995;
http://crunch.ikp.physik.th-darmstadt.de/~wirzba/missing_link.html; further details can be found in M. Reed and B. Simon, *Methods of Modern Mathematical Physics*, Vol. I, Chap VI, Academic Press (New York), 1972; M. Reed and B. Simon, *Methods of Modern Mathematical Physics*, Vol. IV, Chap XIII, Academic Press (New York), 1976.

[38] B. Lauritzen, CHAOS **2**, 409 (1992).

[39] O. Biham and M. Kvale, Phys. Rev. A **46**, 6334 (1992).

[40] K. T. Hansen, Phd–thesis, University of Oslo, (1993).

[41] B. Georgeot and R. E. Prange, Phys. Rev. Lett. **74**, 2851 (1995).

[42] T. Szeredi, J. H. Lefebvre and D. A. Goodings, Nonlinearity **7**, 1463 (1994).

[43] M. R. Haggerty, Phys. Rev. E **52**, 389 (1995).

[44] O. Bohigas, S. Tomsovic and D. Ullmo, Phys. Rev. Lett. **64**, 1479 (1990).

[45] H. P. Baltes and E. R. Hilf, *Spectra of finite systems*, Mannheim: Bibliographisches Institut (1976).

[46] P. W. O'Connor and E. J. Heller, Phys. Rev. Lett. **61**, 2288 (1988).

[47] A. I. Schnirelman, Usp. Mat. Nauk. **29**, 181 (1974); Y. Colin de Verdiere, Commun. Math. Phys. **102**, 497 (1985); S. Zelditch, Duke Math. J. **55**, 919 (1987).

[48] A. Bäcker and H. R. Dullin, *Symbolic Dynamics and Periodic orbits for the Cardiod Billiard*, preprint DESY report DESY 95-198 (November 1995).

[49] H. Bruus and N. D. Whelan, Nonlinearity **9**, 1023 (1996).

[50] G. Tanner and D. Wintgen, Chaos **2**, 53 (1992); G. Tanner and D. Wintgen, Chaos, Solitons & Fractals **5**, 1325 (1995).

[51] P. Cvitanović und B. Eckhardt, J. Phys. A **24**, L237 (1991).

[52] P. Cvitanović and G. Vattay, Phys. Rev. Lett. **71**, 4138 (1993).

[53] P. Dahlqvist, J. Phys. A, **27**, 763 (1994); P. Dahlqvist, Nonlinearity, **8**, 11 (1995).

[54] J. H. Hannay and A. M. Ozorio de Almeida, J. Phys A **17**, 3429 (1984).

[55] P. Cvitanović, K. Hansen and G. Vattay, *Beyond the periodic orbit theory*, preprint (1996).

[56] M. V. Berry, Proc. R. Soc. **400**, 229 (1985).

[57] A. V. Andreev and B. L. Altshuler, Phys. Rev. Let. **75**, 902 (1995); O. Agam, B. L. Altshuler and A. V. Andreev, Phys. Rev. Lett. **75**, 4389 (1995); A. V. Andreev, O. Agam, B. D. Simon and B. L. Altshuler, Phys. Rev. Lett. **76**, 3947 (1996).

[58] E. B. Bogomolny and J. P. Keating, Phys. Rev. Lett. **77**, 1472 (1996).

[59] H. Primak, H. Schanz, U. Smilansky and I. Ussishkin, *Diffraction Effects in the Quantization of Concave Billiards*, preprint, (1996).